

An Equilibrium Dark Matter Halo with the Burkert Profile

Wen-Hao LIU

*Department of Astronomy, Nanjing University, Nanjing, 210093, China
dracoliu@hotmail.com*

Yan-Ning FU

*Purple Mountain Observatory, Chinese Academy of Sciences, Nanjing 210008, and
National Observatories, Chinese Academy of Sciences, Beijing 100039, China*

fyn@pmo.ac.cn

Zu-Gan DENG

*Department of Physics, Graduate School, Chinese Academy of Sciences, Beijing 100039, China
dzg@vega.pku.bac.ac.cn*

and

Jie-Hao HUANG

*Department of Astronomy, Nanjing University, Nanjing 210093, China
jhh@nju.edu.cn*

(Received 2005 April 6; accepted 2005 May 29)

Abstract

In this paper a prescription for generating an equilibrium spherical system depicted with cuspy density profiles is extended to a core density profile, the Burkert profile, which is observationally more suitable to dwarfs. By using a time-saving Monte Carlo method instead of N-body simulations, we show that the Burkert halo initialized with the distribution function that depends only on energy is in a practically stable equilibrium. The one generated using the local Maxwellian approximation is unstable, where the flat core density structure tends to steepen. This is fundamentally different from the previous study on a halo with cuspy density profile. The deviation of the unstable "Burkert" from the initial Burkert profile is found to be closely related to taking a Gaussian as the velocity distribution at any given point. The significance of not using the local Maxwellian approximation is further demonstrated by exploring the dynamical evolution of compact super star clusters in the Burkert halo. In particular, the local Maxwellian approximation will result in underestimating the dynamical friction and overestimating sinking time scale. Accordingly, it will lead to lower probability of forming massive bulges and young nuclear star clusters in bulgeless galaxies.

Key words: cosmology: dark matter - galaxies: kinematics and dynamics - meth-

ods: numerical

1. Introduction

Generating initial conditions for numerical experiments of a system with a certain density profile is a well-defined but difficult procedure. There are two steps for constructing the initial conditions of one desired model: 1) calculate the steady-state distribution function of the desired model; 2) use Monte Carlo method to generate the initial conditions. The main difficulty comes from the first step. One possibility is to make some simplifying approximations about the nature of the distribution function (Toomre, & Toomre 1972; Hernquist & Quinn 1988). Hernquist (1993) described a prescription for constructing N-body realization assuming that velocity distribution at any given point is Maxwellian. It is called the local Maxwellian approximation (Kazantzidis, Magorrian & Moore 2004), of which the advantage is easy to implement. However, Kazantzidis, Magorrian & Moore (2004, KMM hereafter) show that the halo initialized using the local Maxwellian approximation (the Maxwellian halo hereafter for simplicity) can be significantly far from equilibrium, and that for high resolution simulations it is more reasonable to use a stable system generated with a certain steady-state distribution function (the DF halo hereafter).

In particular, they demonstrated that an unstable cuspy halo constructed using the local Maxwellian approximation will soon lose its cusp structure due to its own evolution, which is previously claimed to be due to minor merger between a host halo and the falling sub-system. On the contrary, a stable cuspy halo survives the minor merger. This investigation indicates that the non-equilibrium Maxwellian halo will surely lead to spurious evolution of the host halo when dealing with the response, e.g. the responding of a host halo to sinking SSCs will otherwise be mixed with the artificial evolution of the host halo, induced by its instability. This effect has been investigated in our recent work on the bulge formation in late-type spirals (Fu et al 2005).

The halos on which KMM studied are those with cuspy structure. They have not explored the halos with flat inner profile, e.g. the Burkert profile. The progress in observations (e.g. Marchesini et al. 2002; and the references therein) shows, however, that the cuspy DM profiles, such as the NFW (Navarro, Frenk & White 1997) profile, are not adequate for a large fraction of dwarf galaxies, which are dominated by DM halos, and suggests that the core density profiles, the Burkert (1995) profile for example, are more suitable to these galaxies.

It would then be very much instructive to extend KMM's study to the Burkert halo. It is the halo that contains less mass in the central region than those in the cuspy halos, e.g. the NFW profile. It follows that the technical difficulties will arise for high-resolution simulations of the core halos, especially for those studies focused on the central regions (Fu, Huang &

Deng 2003a; Huang, Deng & Fu 2003). For a given mass of DM halo, our test shows that in order to reach the same resolution in the central $10pc$ region the number of particle for the Burkert halo should be a hundred times more than that for the NFW halo. It would need much more computing time with the N-body simulations.

In this paper, we aim at describing the way to generate the initial conditions for an isotropic, spherical Burkert halo, and perform simulations using the Monte Carlo method (Hénon 1971a,b) to study the stable situation of the Maxwellian and the DF Burkert halos. This may have important implications for the dynamical evolution of SSCs in a responding dark matter halo, resulting in different bulge formation history in late-type spirals.

The organization of the paper is as follows. The procedure to constructing the initial conditions for our model is described in section 2. Section 3 gives the results of the simulations. We discuss the results and illustrate the important implications of generating the DF halo in Section 4. Finally, Section 5 notes our conclusion.

2. Models and Methods

2.1. Density Profile

Here we study the Burkert dark matter halo (1995):

$$\rho = \frac{\rho_s}{(1 + r/r_s)[1 + (r/r_s)^2]} \quad (1)$$

where the central density ρ_s is taken to be $0.05M_\odot/pc^3$ following Marchesini et al. (2002), and the scale radius, r_s is computed from the mass of the DM halo $M_{200} = 10^{11}M_\odot$. In the inner part of the Burkert halo the profile has a core structure, while the slope approximates to -3 in the infinity. The cumulative mass profile with such a distribution diverges as $r \rightarrow \infty$. In fact, the Burkert profile is a phenomenological formula, which provides a good fit to the observed data to less than the virial radius r_{vir} and not valid to arbitrarily large distance from the galactic center. Instead of truncating the profile sharply at r_{vir} , we have chosen an exponential cut-off for $r > r_{vir}$ following KMM, which sets in at r_{vir} and turn-off in a scale r_{decay} .

$$\rho = \frac{\rho_s}{(1 + c)(1 + c^2)} \left(\frac{r}{r_{vir}}\right)^\alpha \exp\left[-\frac{r - r_{vir}}{r_{decay}}\right] \quad \text{for}(r > r_{vir}) \quad (2)$$

where $c \equiv r_{vir}/r_s$ is the concentration parameter. In order to ensure a smooth transition between eq.(1) and eq.(2) at r_{vir} , we require the logarithmic slope there to be continuous. This leads to

$$\alpha = \frac{3r_{vir}}{r_{decay}} - \frac{2c^2}{1 + c^2} - \frac{c}{1 + c} \quad (3)$$

We consider the simulations between a minimum radius r_{min} and a maximum radius r_{max} . The minimum radius is chosen such that it has sufficient particles for us to analyze; The maximum radius is equal to the virial radius plus several r_{decay} . Here we adopt three r_{decay} ($r_{decay} = 0.1r_{vir}$). In addition, we add a boundary at the maximum radius. If the halo is stable, it is in homeostasis,

that is, at any time the number of particles which move out off the boundary is equal to that of particles which move in. In the case of the Burkert halo, the DF (Burkert) halo will not be stable in the outer region, if not adding such a boundary. This is because, not like the case of KMM, the mass outside $r_{vir+3r_{decay}}$ is still not negligible. In other words, a sharp truncation there will make the DF halo unstable.

2.2. Distribution Function

In this paper, we restrict our models to isotropic, non-rotating halos. According to the Jeans' theorem (Lynden-Bell 1962; Binney & Tremaine 1987), the distribution function of any steady-state spherical system can be expressed as $f(E, \mathbf{L})$, where E is the binding energy and \mathbf{L} is the angular momentum vector. As usual, the relative potential Ψ and the relative energy ε (a dimensionless energy in units of $\pi^2 G \rho_s r_s^2$) are defined as:

$$\Psi \equiv -\Phi + \Phi_0; \varepsilon \equiv -E + \Phi_0 \quad (4)$$

where Φ is the potential and Φ_0 is a constant fulfilling $f > 0$ for $\varepsilon > 0$ and $f = 0$ for $\varepsilon \leq 0$. In an isotropic spherical model the distribution function depends on ε only, that is, $f = f(\varepsilon)$. Integrating f over all velocities, we can get the density profile:

$$\rho(r) = \int f(\varepsilon) d^3 \mathbf{v} = 4\pi \int_0^\Psi f(\varepsilon) \sqrt{2(\Psi - \varepsilon)} d\varepsilon \quad (5)$$

The inversion of the above equation gives the distribution function (Eddington 1916; Binney & Tremaine 1987),

$$f(\varepsilon) = \frac{1}{\sqrt{8\pi^2}} \left[\int_0^\varepsilon \frac{d^2 \rho}{d\Psi^2} \frac{d\Psi}{\sqrt{\varepsilon - \Psi}} + \frac{1}{\sqrt{\varepsilon}} \left(\frac{d\rho}{d\Psi} \right)_{\Psi=0} \right] \quad (6)$$

The $d^2 \rho / d\Psi^2$ factor can be evaluated from eq.(1) and eq.(2). The second term of the right-hand side vanishes in large distance in our model.

2.3. Initialization Procedure

Here we describe two approaches to initialize the numerical simulations for the Burkert profile using the local Maxwellian approximation and the steady-state distribution function, respectively.

2.3.1. Exact Distribution Function

Having the density profile $\rho(r)$, we can calculate the model's cumulative mass distribution $M(r)$ and the gravitational potential $\Phi(r)$. Then we can calculate the distribution function from eq.(6).

The integrand in eq.(6) diverges at one or both of the limits, but this can be solved using standard techniques for improper integral (Press et al 1986). The distribution function is obtained on a grid of ε equally spaced in $\log(\varepsilon)$. The accuracy of the numerical integration is checked by comparing the density profile derived from eq.(5) and that given by eq.(1). The

two profiles are very well accordant. We find that the distribution function is non-negative everywhere, which proves that the assumption of the isotropic velocity distribution for the spherical Burkert model is reasonable and physical.

The procedure to obtain the physical quantities of the sampling particles is the following. We randomly sample the initial positions and velocities of the particles. For our model, the probability density function (Windrow 2000) of the particle having the relative energy ε at the radius R is:

$$P(\varepsilon, R) \propto R^2(\Psi(R) - \varepsilon)^{1/2} f(\varepsilon) \quad (7)$$

We use the rejection method (Press et al 1986) to sample the particles in two steps: 1) Generate the position of the particle. The probability density function with radius R is:

$$P(R) \propto R^2 \rho(R) \quad (8)$$

2) Generate the energy of the particle. Once given R , we can get the relative potential $\Psi(R)$. Then the probability density function having the relative energy ε and potential $\Psi(R)$ is:

$$P(\varepsilon) \propto (\Psi(R) - \varepsilon)^{1/2} f(\varepsilon) \quad (9)$$

Once the position R and the relative energy ε of a particle are given, the speed v can be easily determined by $\varepsilon = v^2/2 + \Psi$. Finally, the tangential and radial velocities of each particle can be randomly sampled considering that our model is isotropic.

2.3.2. Local Maxwellian Approximation

The way to sample the position of a particle is the same as that depicted above. The difference is how to generate the velocity of the particle. The collisionless Boltzmann equation for a spherical system can be written as:

$$\frac{d(\rho \overline{v_r^2})}{dr} + \frac{\rho}{r} [2\overline{v_r^2} - (\overline{v_\theta^2} + \overline{v_\phi^2})] = -\rho \frac{d\Phi}{dr} \quad (10)$$

where $\overline{v_r^2}$, $\overline{v_\theta^2}$, and $\overline{v_\phi^2}$ are the velocity dispersions in spherical coordinates (Binney & Tremaine 1987). Assuming the model is isotropic, it can be integrated to:

$$\overline{v_r^2} = \frac{1}{\rho(r)} \int_r^\infty \rho(r) \frac{d\Phi}{dr} dr \quad (11)$$

Using the known density profile, the radial dispersion can be computed as a function of radius. In the local Maxwellian approximation, the 1D velocity distribution at a given point is approximated by a Gaussian (Hernquist 1993):

$$F(v, r) = 4\pi \left(\frac{1}{2\pi\sigma^2} \right)^{3/2} v^2 \exp(-v^2/2\overline{v_r^2}) \quad (12)$$

The speed of a halo particle is initialized from the eq.(12). Then the tangential and radial velocities are randomly sampled in the same way as that described in the above subsection.

2.4. Simulations and Parameters

Many approaches have been used in simulations to study the galactic dynamics. One is to give the statistical description of the system, e.g. distribution function $f(\vec{r}, \vec{v}, t)$. Rosenbluth et al. (1957) discussed a way to calculate f by solving a much complicated equation, Fokker-Planck equation. But it needs to make a number of arbitrary simplifications. A commonly used alternative way is N-body simulations. Unfortunately, this approach requires much computing time, which will greatly increase with the number of particles. As we mentioned before, in the case of a core halo like the Burkert one (1995), a large number of particles are in demand to keep high resolution in the central region. In view of this, we adopt a time-saving method, the Monte Carlo procedure (Henon 1971a,b), rather than the N-body simulations. This procedure has been proved to reproduce the behavior of the system given by the Fokker-Planck equation and to be much faster than the N-body simulations.

The basic ideas of the Monte Carlo procedure is the following. We can divide the gravitation field of the system into two parts: a main smoothed-out field and a small fluctuating one. The particle moves during every time step Δt which satisfies:

$$T_c \ll \Delta t \ll T_r \quad (13)$$

where T_c and T_r are the crossing time and the relaxation time, respectively. The halo evolves accordingly. The relaxation time is related to the crossing time (Binney & Tremaine 1987):

$$T_r/T_c \propto N/\ln N \quad (14)$$

And the crossing time can be calculated as a function of the total mass M and the total energy ε of the system (van Albada 1968):

$$T_c = CGM^{5/2}|\varepsilon|^{-3/2} \quad (15)$$

where C is a numerical constant.

Neglecting the fluctuating field in a first approximation, the motion of the particle is governed by the main spherical symmetry field which changes with the density or mass distribution of the halo. The particle will then take a plane rosette motion (Binney & Tremaine 1987). In any given state the particle is characterized by its position, energy and its angular momentum. One could derive the statistic of the system by randomly choosing the new positions and velocities of the particles on their respective orbits. Taking them as the new conditions, we can calculate a new density (or mass) distribution and accordingly a new potential of the system, which will in turn determine the positions of particles at the next step. The equilibrium state of the halo can be tested by comparing the new density (or mass) distribution with the initial one. Due to this character, if we find some deviation from the initial state of a system at one step, the deviation should grow in the simulations until the system relaxes to a new stable equilibrium (as Figure 1b shows). In other words, what we could illustrate with the Monte Carlo method at the present time is that the system is practically stable or unstable.

Table 1. Parameters of Simulations

Model	M_{total} M_{\odot}	ρ_s M_{\odot}/pc^3	r_s kpc	r_{vir} kpc	r_{max} kpc	N	initializing method
A	10^{11}	0.05	4.0	91.24	118.2	2×10^6	exact distribution function
B	10^{11}	0.05	4.0	91.24	118.2	2×10^6	local Maxwellian approximation

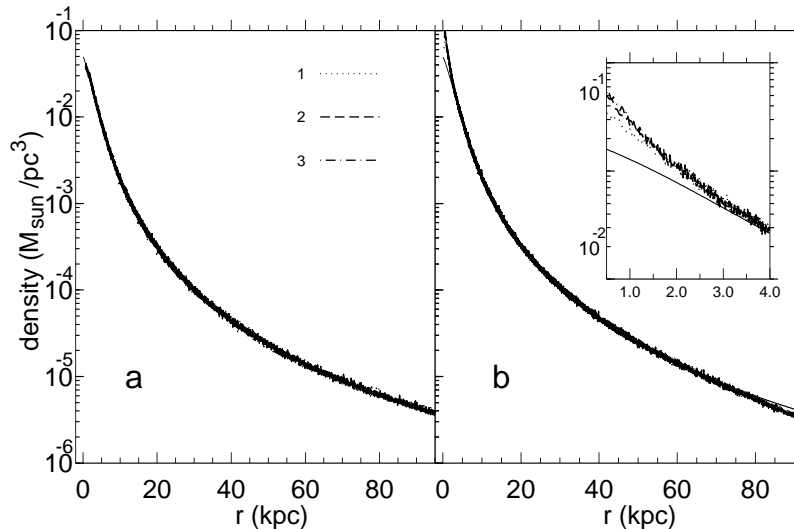


Fig. 1. Radial density profiles for Model A and B are presented in a) and b) panel, respectively. The dotted, dashed and dot-dashed lines in both panels correspond to the density distributions derived at three randomly choosing steps. The thin solid lines in two panels show the initial Burkert profile given by eq.(1). The insert diagram in b) illustrates the situation in the central region for clarity.

For our simulations, the relaxation time of the system is much long and we need not consider the two-body relaxation in our study. If the system is in stable equilibrium, the statistic of the system such as the potential field (or the density and mass distribution) will keep the same though the positions and velocities of the particles are randomly chosen in each step. On the contrary, in an unstable system, from the density or mass profile we can know that the statistic of the system have changed after one step.

The parameters of our simulations are given in Table 1.

3. Results

We run our models for 20 steps and generate 20 individual snapshots. The radial density profiles shown in this section are obtained by binning the particles from individual snapshot. Figure 1a) illustrate the radial density profiles for Model A, where the density distributions at three different steps, denoted with dotted, dashed and dot-dashed lines, are plotted. For

comparison, the (initial) Burkert profile given by eq.(1) is also shown in the figure, denoted with thin solid line. Obviously the radial density profiles for Model A have no evolution over the simulations, all of them are indeed very well matched to the (initial) Burkert profile. In view of this, we conclude that the DF Burkert halo, i.e. the Burkert halo initialized with the exact distribution function, is in stable equilibrium.

The opposite situation occurs for Model B. We present the results in Figure 1b), where the density distributions derived at three randomly choosing steps are indicated. The profiles denoted with dotted, dashed and dot-dashed lines illustrate significant deviation from the (initial) Burkert profile at the central and outer regions. The central distribution tends to steepen as clearly shown in the insert diagram of Figure 1b) and the outer densities decline. The disparity from the initial one simply shows that the Maxwellian Burkert halo, i.e. the Burkert halo generated with the local Maxwellian approximation is not in equilibrium.

4. Discussions

Following KMM, we analyze the actual velocity structure at various distances for Model A, compared with the corresponding Gaussian distributions used in the Maxwellian approximation (Model B). The solid and dotted lines in Figure 2 correspond to the true and Gaussian velocity distributions, respectively, at four different distances from the center. It is evident that only at about the scale radius the Gaussian distribution is a close approximation to the reality. The disparity in the velocity structure from the Gaussian distribution is very strong near the center. The true velocity distributions there are strongly peaked than a Gaussian. It is still apparent at far from the center, where the true velocity structure is shallower than a Gaussian on the contrary.

The feature in velocity distributions described above is indeed reflected in the Maxwellian Burkert halo, where the deviation from the (initial) Burkert halo is obvious at the central and outer regions. The calculations show that the total energy and angular momentum of particles in the Maxwellian Burkert halo are less than those in the DF Burkert halo, i.e. the (initial) Burkert halo. That is, the Maxwellian Burkert halo is colder than the DF Burkert halo. This explains the hoist of the central density profile in the Maxwellian halo. In other words, the unstable situation of the Maxwellian halo is closely related to taking a Gaussian as the velocity distribution at any given point.

In some existing N-body simulations, the considered system with a predetermined mass density profile are initialized using the Maxwellian approximation. In order to start simulations with a system in stable or quasi-stable equilibrium, the authors allow the constructed system to relax for some time so that a certain quasi-stable equilibrium is attained. According to KMM's investigation and the study presented in this work, however, the simulations should start with a system not having the predetermined mass density profile. That is to say, spurious "evolution" of the system initialized with the Maxwellian approximation still cannot be avoided in their

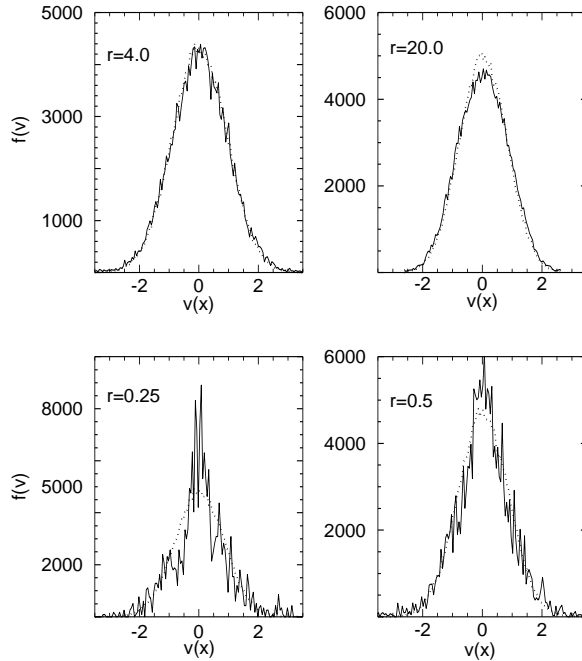


Fig. 2. Histograms of the one dimensional velocity distribution at four different distances from the center in units of *kpc*. The solid lines correspond to the true velocity distribution, and the dotted lines show the Gaussian velocity profile.

way.

Here we would like to further demonstrate the significance of initializing a system with the distribution function by exploring the dynamical evolution of a compact super star cluster (SSC hereafter) in a DM dominated galaxy, depicted with the Burkert profile. The term "compact" here means no tidal stripping is effected. In this case, the most important process involved is the dynamical friction the compact SSC experiences, which reads as (Binney & Tremaine 1987)

$$\frac{d\mathbf{V}_M}{dt} = -16\pi^2 \ln \Lambda G^2 m (M + m) \frac{\int_0^{V_M} f(v_m) v_m^2 dv_m}{V_M^3} \mathbf{V}_M \quad (16)$$

where

$$\Lambda = \frac{b_{max} V_{typ}^2}{G(M + m)} \quad (17)$$

M and V_M (with $V_M = |\mathbf{V}_M|$) are, respectively, the mass and velocity of the SSC experiencing the dynamical friction. The mass of the DM particle, m , is much smaller than M . The quantity b_{max} is the maximum impact parameter and V_{typ} a typical speed. Neither b_{max} nor V_{typ} is precisely defined. Following Binney & Tremaine (1987), we take $b_{max} \equiv 2$ kpc and $V_{typ} \equiv V_M$.

If the DM has a Maxwellian velocity distribution with dispersion σ_{bkqd} , the dynamical friction can be written as:

$$\frac{d\mathbf{V}_M}{dt} = -\frac{2\pi \log(1 + \Lambda^2) G^2 M \rho}{V_M^3} \left[\text{erf}(X) - \frac{2X}{\sqrt{\pi}} \exp(-X^2) \right] \mathbf{V}_M \quad (18)$$

where erf is the error function, and

$$X \equiv \frac{V_M}{\sqrt{2}\sigma_{bkgd}} \quad (19)$$

The velocity dispersion σ_{bkgd} can be evaluated from the Jeans equation.

Eq.(16) and eq.(18) are, respectively, the basis for considering the dynamical friction in the DF Burkert halo and the Maxwellian Burkert one. The initial SSC is assumed to move at a radius $r=1\text{kpc}$ with the local circular velocity. The sinking history of the SSC is presented in Figure 3 a) and b) for SSC with different masses. The thick solid lines in both panels express the case in Model A, i.e. in the Burkert halo initialized using the distribution function, while the thick dotted lines the case in Model B, i.e. in the Maxwellian Burkert halo.

We can see from Figure 3a) that the SSC with typical mass of $2 \times 10^6 M_\odot$ (Fu, Huang & Deng 2003a) sinks quickly, in about $4 \times 10^8 \text{yr}$, to the central region within a hundred pc in Model A, while takes much longer time in Model B. It means that the SSC in Model A experiences much stronger dynamical friction and loses angular momentum quickly at first. This situation is consistent with the velocity distributions that we discussed above. In fact, in an isotropic halo, the effect of the dynamical friction comes from the DM particles whose velocities are less than that of the SSC (Binney & Tremaine 1987). As we illustrated in Figure 2, the true velocity structure in the inner part of the halo is more peaked than a Gaussian. Thus more particles with low velocities exist, resulting in stronger dynamical friction on SSC. Inside 200 pc from the center, the SSC in Model A sinks slowly than that in Model B, mainly due to its low velocity and low deceleration accordingly.

A similar sinking story is presented in Figure 3b) for a SSC with mass of $8 \times 10^5 M_\odot$, where we can find same trend of faster sinking in Model A than in Model B. The interesting thing is that the SSC with smaller mass reaches the center, less than 10 pc , in shorter period of time, as compared with the corresponding situation in Model A shown in Figure 3a). The compact SSC with larger mass experiences stronger dynamical friction, resulting in stronger deceleration but longer sinking time.

As we know, when the dynamical friction exists the periodic motion of a test particle in a spherical potential is damped like that of a damped simple harmonic oscillator. If the dynamical friction is strong enough, it is possible for the motion to lose completely its oscillation behavior, the so-called over-damping. For an over-damped SSC, the energy of SSC is in the form of potential energy in most of time, which makes the energy loss by dynamical friction much less effective than otherwise. For an incompact SSC, the tidal stripping must not be ignored. In that case, the peeling process will make a heavy SSC lighter, and the over-damping may not appear.

The shorter sinking time for SSCs in a DM halo initialized with the steady-state distri-

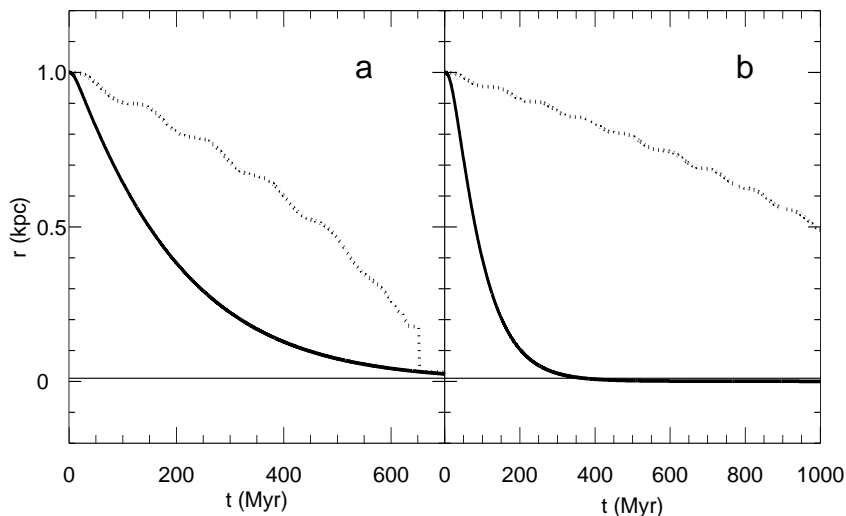


Fig. 3. Sinking history of a compact SSC in the Burkert halo. Panel a) and b) present the situation for SSC with mass of $2 \times 10^6 M_\odot$ and $8 \times 10^5 M_\odot$, respectively. The thick solid lines in both panels correspond to the case in Model A, i.e. the Burkert halo initialized with the distribution function, while the thick dotted ones in Model B: the Maxwellian halo. The thin solid line denotes the distance of 10 pc to the center

bution function should lead to higher probability of forming massive bulges in late-type galaxies (Fu, Huang & Deng 2003a), as well as of forming nuclear star clusters at young ages (Huang, Deng & Fu 2003). It will also bring the intermediate mass black holes, the seed black holes, within SSCs to the center of a DM halo at early stage (Fu, Huang & Deng 2003b). All of these matter are hot topics in astrophysics, which emphasizes the important implications of using the distribution function to initialize the system.

5. CONCLUSION

Constructing appropriate and reasonable initial conditions for an isolated equilibrium system is one of the most important points to various numerical simulations related to the formation and evolution of galaxies. In this paper, we extend KMM’s study on cuspy density profiles to the Burkert profile. Using a time-saving Monte Carlo method, we have shown clearly that the Burkert halo initialized with the local Maxwellian approximation tends to steepen, which is closely related to adopting a Gaussian as the velocity distribution at any given points. This spurious evolution leads to underestimating the dynamical friction on SSCs moving in dark matter dominated galaxies. This important demonstration gives us a valuable clue to clarify the embarrassed situation in our previous investigation (Fu, Huang & Deng 2003a; Huang, Deng & Fu 2003), i.e. the adopted Maxwellian approximation in these works causes longer sinking time for SSCs so as not to form massive bulges in a few Gyrs and not to form a young nuclear star cluster in the Burkert halo. To initialize the dark matter halos with the steady-

state distribution function should be critical to what we are pursuing, as what we have shown in this paper.

The authors would like to thank the referee, Andi Burkert, for his valuable comments which improve the description of the paper. This work is supported by NKBRFSF G19990754 and NSFC 10373008. Fu is partly supported by the NSFC 10233020.

References

- Binney, J., & Tremaine, S. 1987, *Galactic Dynamics* (Princeton: Princeton University Press)
- Burkert, A. 1995, *ApJ*, 447, L25
- Eddington, A.S. 1916, *MNRAS*, 76, 572
- Fu, Y.N., Huang, J.H., Deng, Z.G. 2003a, *MNRAS*, 339, 442
- Fu, Y. N., Huang, J. H., & Deng, Z. G. 2003b, *Carnegie Obs. Astrophys. Ser.*, Vol. 1: *Coevolution of Black Holes and Galaxies*, ed. L. C. Ho (Pasadena: Carnegie Observatories),
- Fu, Y.N., Liu, W.H., Deng, Z.G., & Huang, J.H. 2005, to be submitted
- Henon, M. 1971a, *ApSS*, 13, 284
- Henon, M. 1971b, *ApSS*, 14, 151
- Hernquist, L. 1993, *ApJS*, 86, 389
- Hernquist, L., & Quinn, P.J. 1988, *ApJ*, 331,682
- Huang, J.H., Deng, Z.G. Fu, Y.N. 2003, *PASJ*, 55, L89
- Kazantzidis, S., Magorrian, J., & Moore, B. 2004, *ApJ*, 601,37 (KMM)
- Lynden-Bell, D. 1962, *MNRAS*, 214, 1
- Marchesini, D., D'Onghia, E., Chincarini, G., Firmani, C., Conconi, P., Molinari, E., & Zacchei, A. 2002, *ApJ*, 575, 801
- Navarro, J.F., Frenk, C.S. & White, S.D.M. 1997, *ApJ*, 490, 493
- Press, W.H., Flannery, B.P., Teukolsky, S.A., & Vetterling, W.T. 1986, *Numerical Recipes*, Cambridge University Press.
- Rosenbluth, M.N., MacDonald, W.M., & Judd, D.L. 1957, *Phys. Rev.*, 107, 1
- Toomre, A., & Toomre, J. 1972, *ApJ*, 178,623
- Windrow, L.M. 2000, *ApJS*, 131, 39
- van Albada, T.S. 1968, *BAIN*, 19,479